Editors' Suggestion Featured in Physics

New Plasma Regime in Jupiter's Auroral Zones

R. L. Lysak,[1,*] A. H. Sulaiman,[1] S. S. Elliott,[1] W. S. Kurth,[2] and S. J. Bolton[3]
[1]*School of Physics and Astronomy, University of Minnesota, Minneapolis, Minnesota, USA*
[2]*Department of Physics and Astronomy, University of Iowa, Iowa City, Iowa, USA*
[3]*Southwest Research Institute, San Antonio, Texas, USA*

(Received 14 March 2025; accepted 27 May 2025; published 16 July 2025)

Observations from the Juno satellite have indicated very low electron densities, as low as 10^{-3} cm^{-3}, at high-latitudes in Jupiter's magnetosphere. This region is strongly magnetized, with surface magnetic fields at the one-bar level up to 20 G, or 2 mT, leading to the unusual situation that the electron plasma frequency is less than the ion gyrofrequency. In this extremely low-density plasma, the Alfven wave becomes a plasma oscillation at the electron plasma frequency at shorter perpendicular wavelengths. Analysis of this mode with a kinetic low-frequency dispersion solver indicates that at large wave number, this mode has the characteristics of the Langmuir wave. Thus, this mode can be called an Alfvén-Langmuir mode. Below the plasma frequency, the high-wave number behavior of this mode exhibits a resonance cone, with frequency determined by the angle of the wave vector with the background magnetic field. These waves can be excited by the upward electron beams observed by Juno.

DOI: 10.1103/fn63-qmb7

Introduction—Observations of the cutoffs and resonances of plasma wave modes have proven to be an effective means of determining the electron density of a plasma [1–8]. Such wave measurements are often a more reliable measure of the plasma density than are direct particle measurements, since particle detectors necessarily have a limited energy range and count rate and are affected by the spacecraft potential. Measuring the plasma frequency determines the electron density without these limitations.

The Juno spacecraft is in a polar orbit around Jupiter with perijove at 3500 km, or 1.05 R_J (1 R_J = 71 492 km, the equatorial 1-bar radius of Jupiter). During Juno's extended mission, the precession of the orbit has caused the perijove to move toward the north pole of Jupiter, leading to multiple passes over the low-altitude Jovian polar regions. The Waves instrument on Juno [4] measures electric fields from 50 Hz to 40 MHz and magnetic fields from 50 Hz to 20 kHz, ranges that encompass many of the relevant wave cutoffs and resonances. Using these techniques, Sulaiman *et al.* [6] showed that the densities in the main Zone I auroral region [9] dropped to values of 10^{-2} cm^{-3}. These values were shown to be consistent with measurements from the JADE particle instrument on Juno [10]. As Juno passes over the pole, the densities can drop further, reaching values of 10^{-3} cm^{-3} [1].

As is well known, the electron plasma frequency can be estimated by $f_{pe} = 9$ kHz$\sqrt{n}$, where the density is measured in electrons/cm^3. Thus, at these low densities, the plasma frequency can be less than 1 kHz. Moreover, the polar regions at Jupiter contain very large magnetic fields. At the one-bar level of Jupiter, the magnetic field can reach a magnitude of 20 G, or 2 mT [11]. As a reference point, the proton gyrofrequency is about 1.5 kHz B, where B is measured in Gauss, corresponding to the electron plasma frequency for a density of 0.03 cm^{-3}. This implies that this plasma has the unusual property that the electron plasma frequency is less than the ion cyclotron frequency. As we will show below, this leads to a new plasma mode that does not exist in a typical plasma. It should be emphasized that plasmas in which the electron plasma frequency is less than the electron cyclotron frequency, often called "underdense" plasmas [12], are often observed and have been connected with the source region for auroral kilometric radiation [13]. However, to our knowledge, the regime where the electron plasma frequency is less than the ion cyclotron frequency has never been observed or analyzed previously.

Figure 1 shows an example of these waves as measured by the Juno Waves instrument. The white line in the top figure gives the proton cyclotron frequency for this event, which is centered around 9 kHz, corresponding to a magnetic field of 6 G (600 μT). The black line gives the upper bound of the wave emissions. The corresponding plasma density is plotted in the lower panel of the figure, giving densities in this case between 0.1 and 1 cm^{-3}.

*Contact author: lysak001@umn.edu

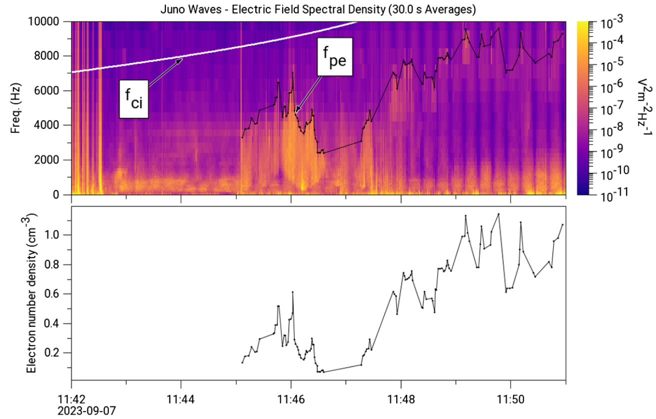

FIG. 1. Top: Amplitude of the electric field fluctuations during a Juno pass over the Jupiter's north pole. The white line indicates the ion cyclotron frequency while the black line gives the electron plasma frequency. Bottom: the inferred density from the plasma frequency measurement.

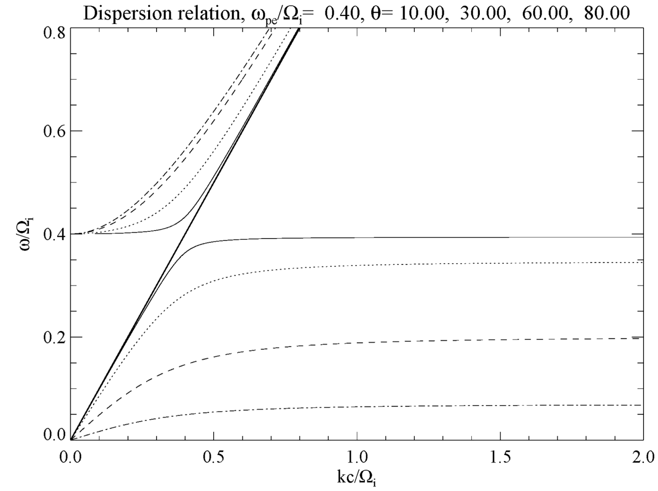

FIG. 2. Plot of the cold plasma dispersion relation for $\omega_p/\Omega_i = 0.4$ at angles of 10° (solid), 30° (dotted), 60° (dashed), and 80° (dash-dot).

The purpose of this Letter is to investigate the dispersion relation of this mode in a strongly magnetized, low-density plasma. The next section will employ the standard cold plasma dispersion relation to investigate the properties of this mode. Then, we will apply a fully kinetic, low-frequency dispersion relation to consider the properties of this mode in a finite temperature plasma and its excitation by electron beams. Finally, we will briefly discuss the possible reasons for such low densities in this region.

Cold plasma dispersion relation—We can start from the standard, cold plasma dispersion relation [14]:

$$\det\begin{pmatrix} S-n_\parallel^2 & -iD & n_\parallel n_\perp \\ iD & S-n_\parallel^2-n_\perp^2 & 0 \\ n_\parallel n_\perp & 0 & P-n_\perp^2 \end{pmatrix}=0, \tag{1}$$

where $n = kc/\omega$, $n_\parallel = n\cos\theta = k_\parallel c/\omega$, $n_\perp = n\sin\theta = k_\perp c/\omega$, and the elements of the dielectric tensor are given by

$$S = 1-\sum_s \frac{\omega_{ps}^2}{\omega^2-\Omega_s^2}, \qquad D = \sum_s \frac{\Omega_s}{\omega}\frac{\omega_{ps}^2}{\omega^2-\Omega_s^2},$$
$$P = 1-\frac{\sum_s \omega_{ps}^2}{\omega^2} = 1-\frac{\omega_p^2}{\omega^2}. \tag{2}$$

Here $\omega_{ps}^2 = n_s q_s^2/\varepsilon_0 m_s$ and $\Omega_s = q_s B/m_s$ are the angular plasma frequency and gyrofrequency, respectively, for species s, and the sums are over all species in the plasma. The standard practice is to solve Eq. (1) for n given an angle θ, which yields a quadratic equation for n^2:

$$An^4 - Bn^2 + C = 0. \tag{3}$$

In this equation, we have

$$A = S\sin^2\theta + P\cos^2\theta,$$
$$B = (S^2-D^2)\sin^2\theta + SP(1+\cos^2\theta),$$
$$C = P(S^2-D^2). \tag{4}$$

Figure 2 shows the results of this dispersion relation for the case when $\omega_{pe}/\Omega_i = 0.4$, consistent with the observations in Fig. 1. The curves in this figure show the dispersion relations for wave vector angles of 10° (solid), 30° (dotted), 60° (dashed), and 80° (dash-dot) with respect to the background magnetic field. The solid line extending from zero frequency to the ion cyclotron frequency gives the standard Alfvén wave, which for parallel propagation has a phase speed almost equal to the speed of light for these low densities. At other angles, the Alfvén waves have a phase velocity equal to $c_A\cos\theta$, where $c_A = c/\sqrt{1+\mu_0\rho c^2/B^2}$ is the Alfvén speed modified by the displacement current. At larger wave number, the frequency depends only on the angle of propagation. According to Eqs. (3) and (4), this frequency is given by $A = 0$ in the limit that $n \to \infty$. For these parameters, this frequency is simply $\omega = \omega_{pe}\cos\theta$, consistent with the results shown in the figure. The branches of the dispersion relation with a cutoff at the plasma frequency for $k = 0$ are O-mode waves that extend to the ion gyrofrequency, and couple to the free space electromagnetic mode.

These waves are likely driven by electrons at the Landau resonance with $v_\parallel = \omega/k_\parallel = c/n_\parallel$ [15]. Therefore, it makes sense to solve the dispersion relation equation (1) for $n_\perp$ at a fixed $n_\parallel$. This leads to a quadratic equation (3) for $n_\perp^2$ rather than n^2, but with the coefficients given by [16,17].

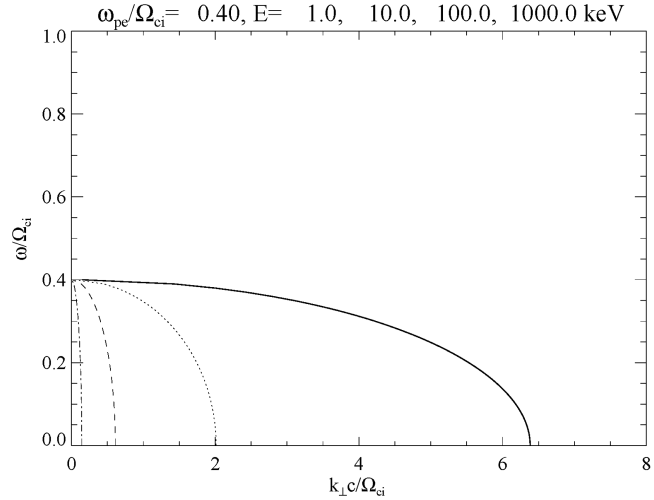

FIG. 3. The dispersion relation plotted for waves with parallel phase velocity corresponding to electron energies of 1 keV (solid), 10 keV (dotted), 100 keV (dashed), and 1 MeV (dash-dot).

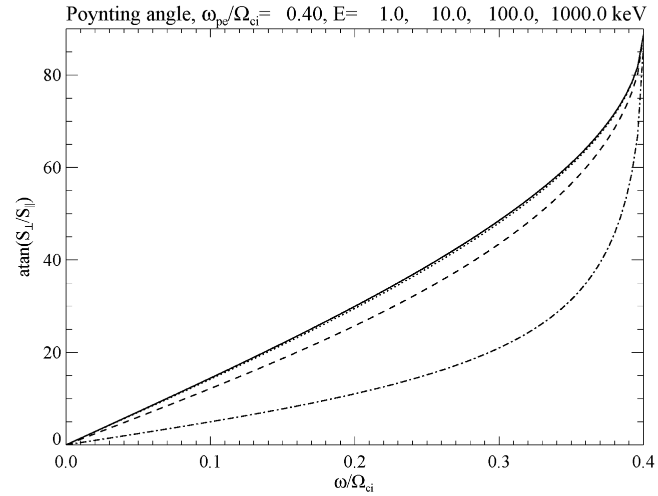

FIG. 4. The angle the Poynting vector makes with the background magnetic field for resonant energies of 1 (solid), 10 (dotted), 100 (dashed), and 1000 keV(dash-dot), as in Fig. 3. The heavy solid curve denotes the angle at the resonance cone. For all energies, the angle is less than the resonance cone angle.

$$A = S, \quad B = S^2 - D^2 + SP - n_\parallel^2(S+P),$$
$$C = P\left[\left(n_\parallel^2 - S\right)^2 - D^2\right]. \tag{5}$$

Figure 3 shows the dispersion relation in this format for resonant electron energies of 1 (solid), 10 (dotted), 100 (dashed), and 1000 keV (dot-dash). Note that the higher frequency branch seen in Fig. 2 is not present in Fig. 3, since those waves have phase velocities greater than the speed of light.

As noted above, the frequency at large wave number becomes a function only of the angle of propagation, forming a resonance cone. In this case, the direction of the group velocity and the Poynting vector also become only a function of the frequency. Figure 4 shows the group velocity angle as a function of frequency for waves with the Landau resonances of 1, 10, 100, and 1000 keV, with the line styles as in Fig. 3. Here the solid curve gives the resonance cone prediction, which indicates the maximum angle with respect to the magnetic field for these waves. It can be seen from this figure that the waves with Landau resonance at the lower energies match the resonance cone prediction, while the larger energies have Poynting vectors more parallel to the background field. This structure leads to a saucerlike lower cutoff when a spacecraft passes over a localized source, as can be seen at 11:46 in Fig. 1. A satellite passing over the source will first see the higher frequency waves that propagate at a large angle to the magnetic field, then the lowest observed wave frequency will decrease, reaching its lowest point when the satellite is directly over the source, after which the frequency will increase again. This feature has often been observed in the whistler resonance cone at Earth [18–22], where they have been called VLF saucers; however, this is the first time this has been reported in this low-frequency mode.

Further properties of the waves are discussed in the Supplemental Material [23].

Kinetic dispersion relation—Next, we will consider the kinetic dispersion relation [24,25]. Under the approximations of for low frequencies, $\omega < \Omega_i$ and short perpendicular wavelength, $k_\perp V_A/\Omega_i = k_\perp c/\omega_{pi} \gg 1$, the fast MHD mode, denoted by the middle row of the dielectric tensor, equation (1), has a frequency $\omega > k_\perp V_A \gg \Omega_i$ and so it decouples from the system. Neglecting the middle row and column, the determinant can be written

$$n_\parallel^2 = S\left(1 - \frac{n_\perp^2}{P}\right). \tag{6}$$

Here the perpendicular response is mainly due to the ions and the parallel response to the electrons, so we have

$$S = 1 + \frac{c^2}{V_A^2} G(\mu_i, \omega/\Omega_i), \quad P = 1 + \frac{\Gamma_0(\mu_e)}{k_\parallel^2 \lambda_D^2}\left(1 + \xi Z(\xi)\right), \tag{7}$$

where $\xi = \omega/k_\parallel a_e$, $\mu_s = k_\perp^2 \rho_s^2$, $a_e = \sqrt{2T_e/m_e}$, $\lambda_D = \sqrt{\varepsilon_0 T_e/ne^2}$, and $\rho_i = \sqrt{m_i T_i}/eB$. The factor G is

$$G = \frac{1 - \Gamma_0(\mu_i)}{\mu_i} + \frac{2\Gamma_1(\mu_i)}{\mu_i}\frac{\omega^2/\Omega_i^2}{1 - \omega^2/\Omega_i^2}. \tag{8}$$

$\Gamma_n(x) = e^{-x} I_n(x)$ is related to the modified Bessel function and $Z(\xi)$ is the plasma dispersion function [26]. After some manipulation, the dispersion relation can be written in the form

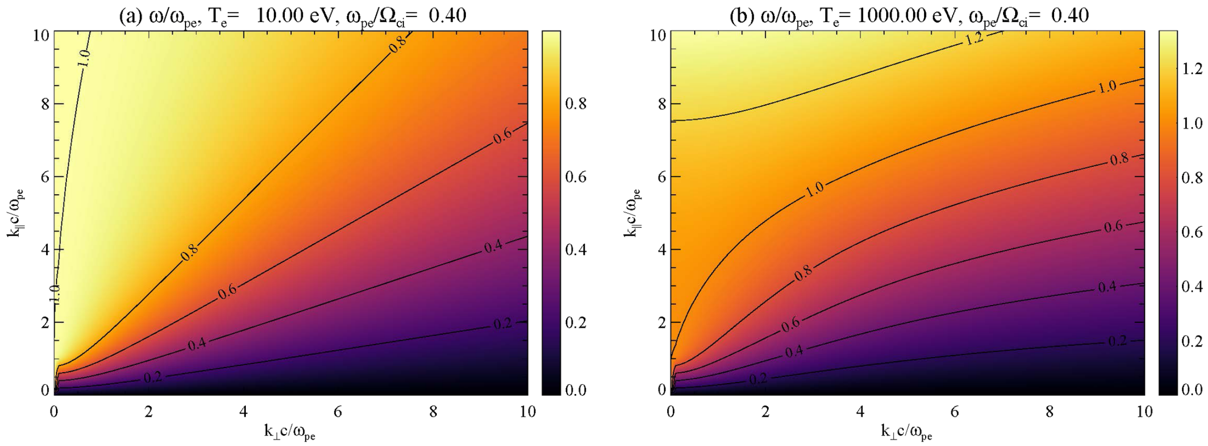

FIG. 5. Kinetic dispersion relation plotted in k space for electron temperatures of (a) 10 and (b) 1000 eV. Contour labels give wave frequencies normalized to the plasma frequency.

$$\left(\frac{\omega}{k_\parallel c}\right)^2 = \frac{1}{1+(c^2/V_A^2)G} + \frac{k_\perp^2\lambda_D^2}{k_\parallel^2\lambda_D^2 + \Gamma_0(\mu_e)(1+\xi Z(\xi))}. \tag{9}$$

The complex roots of this equation are found using Muller's method ([27], Sec. 9.5) as implemented by the IDL routine fx_root.

Figure 5 shows the dispersion relation for a single Maxwellian electron species as a function of the perpendicular and parallel wave numbers for temperatures of (a) 10 and (b) 1000 eV. The 10 eV case is, as expected, virtually identical to the cold plasma result, with the wave frequency staying below the plasma frequency. At this temperature, the frequency depends only on the angle that the wave vector makes with the magnetic field, indicating a resonance cone structure. However, as the electron temperature increases, the wave frequency increases above the plasma frequency at large parallel wave numbers, with the slope of the curves scaling with the electron thermal speed. This is consistent with the usual behavior of the Langmuir wave in a plasma, although usually the Langmuir wave is a narrow band emission at and slight above the plasma frequency [12]. Thus, in this case, the wave has the characteristics of an Alfvén wave at small wave numbers and a Langmuir wave at large wave numbers and so could be called an Alfvén-Langmuir wave. These dispersion relations are presented as line plots in the Supplemental Material [23].

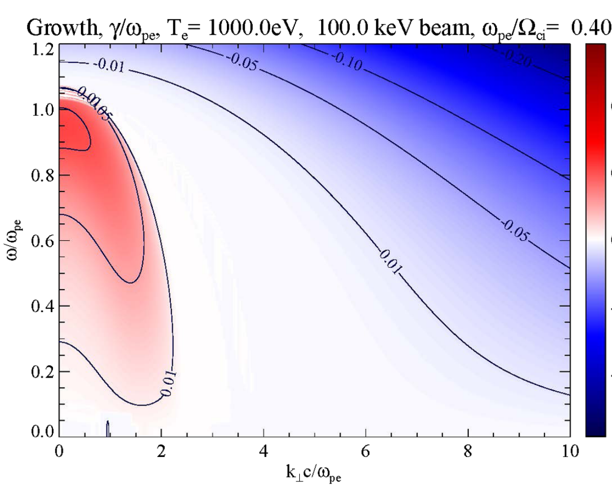

FIG. 6. Growth rate for a 100 keV electron beam passing through a 1 keV temperature plasma as a function of $k_\perp$ and ω. Contours give the growth rate normalized to the plasma frequency.

Beam-plasma instability—Juno observes upward going beams of electrons with energies up to 100 keV [28,29]. As Fig. 3 shows, such electrons will be in Landau resonance with the wave modes described here. To investigate the possibility of wave excitation by such a beam, we have introduced a beam population into the kinetic dispersion relation solver described in the previous section. The beam is modeled by a drifting Maxwellian distribution. Results are shown in Fig. 6 for an electron beam with a drift energy of 100 keV in the presence of a background electron population. The beam density is taken to be 1% of the background population and the beam and background temperatures are both 1 keV. As in the previous figures, the density has been set so that the plasma frequency is 0.4 times the proton cyclotron frequency. These results are consistent with Fig. 3 showing the maximum growth rate is at the location of the Landau resonance. In addition, the maximum growth rate in each case is just below the plasma frequency, consistent with the observations of Fig. 1.

Discussion—The results presented above indicate the existence of a new type of plasma wave mode occurring in the unusual conditions of high magnetic field strength and low plasma density at high latitudes and low altitudes in Jupiter's magnetosphere. The low plasma density is corroborated by the measurements of the O-mode cutoff as well as direct particle measurements [1,7,10]. The results from the dispersion relationship confirm the existence of the waves at frequencies below the plasma frequency. In a warm plasma, the kinetic dispersion relation indicates that the waves can act like the Langmuir wave and propagate just above the plasma frequency, although those waves are damped. In the presence of a beam, the results indicate that the largest growth rates occur just below the electron plasma frequency.

The observation of such low plasma density raises the question of why the density in this region is so low. Global MHD simulations [30] as well as the precipitation of energetic heavy ions from the plasma sheet [9,31,32] suggest that most of the high-latitude magnetosphere is on closed field lines. These field lines map to distances greater than 50 R_J, indicating that the ions must overcome a large magnetic field gradient that reflects them before reaching the lower altitude parts of the field line. A model of the Jovian plasma sheet based on data from the Galileo satellite [33] indicates that the plasma sheet density at 50 R_J is about 0.03 cm^{-3}, consistent with observations from Juno [34]. The presence of such ions at low altitude suggests that they are pitch-angle scattered into the loss cone by electromagnetic ion cyclotron waves [35].

Another source of plasma on polar field lines could be Jupiter's ionosphere. However, the gravitational pull of Jupiter may limit the expansion of Jupiter's ionosphere to high altitudes. Since the gravitational scale height of the electrons is much less than the scale height of the ions, an ambipolar field should be set up. This potential is given by the gravitational potential on the average mass of the plasma, which is roughly half the proton mass, since Jupiter's ionosphere is largely protons and the electrons have negligible mass. Thus the potential difference between the surface of Jupiter and a radial distance r is

$$U = \frac{GM_J m_p}{2R_J}\left(1 - \frac{R_J}{r}\right) = 9.25\ \mathrm{eV}\left(1 - \frac{R_J}{r}\right). \quad (10)$$

In equilibrium, the density will be given by $n = n_0 \exp(-U/T)$. Since the ionospheric temperature is about 1000 K, or roughly 0.1 eV (e.g., [36]), the density will be 0.02 cm^{-3} at 1.2 R_J,. assuming an ionospheric density of 10^5 cm^{-3}. Note one distinction between the polar regions of Earth and Jupiter: at Earth, Oxygen ions dominate up to about 1000 km, and the ambipolar potential is largely set by maintaining the charge balance between the oxygen ions and the electrons. In this case, the lighter protons feel a net upward force, forming the polar wind that populates the polar cap [37]. However, at Jupiter, the protons are the major ion and so the polar cap density remains low.

In spite of the ambipolar potential retarding the motion of the electrons, energetic electron beams, still escape the ionosphere. This could be due to the development of a parallel electric field at very low altitudes. There could be a type of feedback in this region where the initial low density of ionospheric electrons supports the development of parallel electric fields, which in turn accelerate electrons up the field line, further decreasing their density. Another possibility is that the impact of the heavy ions on the ionosphere will lead to the production of secondary electrons, a process that occurs at Earth due to energetic electron precipitation [38,39]. Observations from the Juno extended mission should clarify these issues.

Conclusions—The conditions in Jupiter's polar magnetosphere of high magnetic field and low plasma density give rise to a situation unique among plasma environments visited to date by spacecraft where the electron plasma frequency is less than the ion cyclotron frequency. This gives rise to a new type of wave mode that begins at small wave number as an Alfvén wave and transitions at large wave number to a Langmuir wave. This wave exhibits resonance cone behavior at large wave number with the frequency being only a function of angle, $\omega = \omega_p \cos\theta$.

The results presented here show that this wave branch can be excited at the Landau resonance by electron beams with energies in the 1 keV–1 MeV range. Because of the resonance cone structure, these waves can also exhibit a saucerlike feature when a spacecraft passes over a localized source, which has often been seen in the whistler mode but is reported here for the first time in the Alfvén-Langmuir mode.

Therefore, the low-density, high magnetic field conditions in Jupiter's polar regions support a new plasma mode, the Alfvén-Langmuir wave. While such conditions do not occur at Earth, it is possible that they apply in polar regions of the other giant planets and potentially in strongly magnetized exoplanets or stars.

Acknowledgments—R. L. L. was supported by NASA Grant No. 80NSSC20K1269 and NSF Grant No. AGS-2225270 to the University of Minnesota. A. H. S. at the University of Minnesota is supported by NASA through Contract No. S99022AKP with the Southwest Research Institute. The research at the University of Iowa is supported by NASA through Contract No. 699041X with the Southwest Research Institute. S. S. E. acknowledges the support of internal funds from the University of Minnesota. W. S. K. acknowledges the use of the Space PHYSICS Data Repository at the University of Iowa supported by the Roy J. Carver Charitable Trust. The authors would like to acknowledge Jeremy Faden and the use of Autoplot, which was used to present the data shown.

R. L. L. developed and performed the calculations of the dispersion relation. A. H. S. and S. S. E. analyzed the data from the Juno satellite and noted the unique nature of the data. W. S. K. and S. J. B. provided the Juno data used in this work.

Data availability—The data that support the findings of this Letter are openly available [40].

[1] A. H. Sulaiman, O. Santolik, F. Allegrini, W. S. Kurth, R. L. Lysak, S. S. Elliott *et al.*, Electron densities in Jupiter's polar regions from the identification of ordinary-mode cutoffs, in *Planetary, Solar and Heliospheric Radio Emissions IX*, edited by G. Fischer, C. M. Jackman, C. K. Louis, A. H. Sulaiman, and P. Zucca (2023), 10.25546/103098.

[2] D. A. Gurnett, F. L. Scarf, W. S. Kurth, R. R. Shaw, and R. Poynter, L 630, Determination of Jupiter's electron density profile from plasma wave observations, J. Geophys. Res. **86**, 8199 (1981).

[3] D. A. Gurnett, A. M. Persoon, W. S. Kurth, A. Roux, and S. J. Bolton, Electron densities near Io from Galileo plasma wave observations, J. Geophys. Res. **106**, 26225 (2001).

[4] W. S. Kurth, S. De Pascuale, J. B. Faden, C. A. Kletzing, G. B. Hospodarsky, S. Thaller, and J. R. Wygant, Electron densities inferred from plasma wave spectra obtained by the Waves instrument on Van Allen Probes, J. Geophys. Res. **120**, 904 (2015).

[5] S. S. Elliott, A. H. Sulaiman, W. Kurth, J. Faden, F. Allegrini, P. Valek *et al.*, The high-latitude extension of Jupiter's Io torus: Electron densities measured by Juno Waves, J. Geophys. Res. **126**, e2021JA029195 (2021).

[6] A. H. Sulaiman, S. S. Elliott, W. S. Kurth, J. B. Faden, G. B. Hospodarsky, and J. D. Menietti, Inferring Jovian electron densities using plasma wave spectra obtained by the Juno/Waves instrument. J. Geophys. Res. **126**, e2021JA029263 (2021).

[7] A. H. Sulaiman, B. H. Mauk, J. R. Szalay, F. Allegrini, G. Clark, G. R. Gladstone *et al.*, Jupiter's low-altitude auroral zones: Fields, particles, plasma waves, and density depletions, J. Geophys. Res. **127**, e2022JA030334 (2022).

[8] R. B. Horne, T. A. Daggitt, N. P. Meredith, S. A. Glauert, X. Liu, and L. Chen, Measuring low plasma density in the Earth's equatorial magnetosphere from magnetosonic waves, Geophys. Res. Lett. **51**, e2024GL108407 (2024).

[9] B. H. Mauk, G. Clark, G. R. Gladstone, S. Kotsiaros, A. Adriani, F. Allegrini *et al.*, Energetic particles and acceleration regions over Jupiter's polar cap and main aurora: A broad overview, J. Geophys. Res. **125**, e2019JA027699 (2020).

[10] F. Allegrini, W. S. Kurth, S. S. Elliott, J. Saur, G. Livadiotis, G. Nicolaou *et al.*, Electron partial density and temperature over Jupiter's main auroral emission using Juno observations, J. Geophys. Res. **126**, e2021JA029426 (2021).

[11] J. E. P. Connerney, S. Timmins, R. J. Oliversen, J. R. Espley, J. L. Joergensen, S. Kotsiaros *et al.*, A new model of Jupiter's magnetic field at the completion of Juno's Prime Mission, J. Geophys. Res. **127**, e2021JE007055 (2022).

[12] C. Moser, J. LaBelle, and I. H. Cairns, High bandwidth measurements of auroral Langmuir waves with multiple antennas, Ann. Geophys. **40**, 231 (2022).

[13] R. E. Ergun, C. W. Carlson, J. P. McFadden, F. S. Mozer, G. T. Delory, W. Peria, C. C. Chaston, M. Temerin, R. Elphic, R. Strangeway, R. Pfaff, C. A. Cattell, D. Klumpar, E. Shelley, W. Peterson, E. Moebius, and L. Kistler, FAST observations in the AKR source region, Geophys. Res. Lett. **25**, 2061 (1998).

[14] T. H. Stix, *Waves in Plasmas* (Springer, Berlin 1992).

[15] S. S. Elliott, D. A. Gurnett, P. H. Yoon, W. S. Kurth, B. H. Mauk, R. W. Ebert *et al.*, The generation of upward-propagating Whistler mode waves by electron beams in the Jovian polar regions, J. Geophys. Res. **125**, e2020JA027868 (2020).

[16] R. L. Lysak and M. A. Temerin, Generation of Alfvén-ion cyclotron waves on auroral field lines in the presence of heavy ions, Geophys. Res. Lett. **10**, 643 (2020).

[17] M. Temerin and R. L. Lysak, Electromagnetic ion cyclotron (ELF) waves generated by auroral electron precipitation, J. Geophys. Res. **89**, 2849 (1982).

[18] S. R. Mosier and D. A. Gurnett, VLF measurements of the Poynting flux along the geomagnetic field with the Injun 5 satellite, J. Geophys. Res. **74**, 5675 (1969).

[19] D. A. Gurnett, S. R. Mosier, and R. R. Anderson, Color spectrograms of very-low frequency Poynting flux data, J. Geophys. Res. **76**, 3022 (1971).

[20] H. G. James, VLF saucers, J. Geophys. Res. **81**, 501 (1976).

[21] M. Temerin, C. Cattell, R. Lysak, M. Hudson, R. B. Torbert, F. S. Mozer, R. D. Sharp, and P. M. Kintner, The small scale structure of electrostatic shocks, J. Geophys. Res. **86**, 11278 (1981).

[22] C. Moser, J. LaBelle, S. Hatch, J. I. Moen, A. Spicher, T. Takahashi *et al.*, The cusp as a VLF saucer source: First rocket observations of long-duration VLF saucers on the dayside, Geophys. Res. Lett. **48**, e2020GL090747 (2021).

[23] See Supplemental Material at http://link.aps.org/supplemental/10.1103/fn63-qmb7 for additional information on the dispersion relations for the Alfvén-Langmuir waves, both in the cold plasma limit and from the fully kinetic dispersion relation. This includes the polarization properties of the waves, such as E/B ratio and the Epar/Eperp ratio and the wave normal angle with respect to the background magnetic field. Also included are additional plots of the kinetic dispersion relation wave frequency and growth rate.

[24] R. L. Lysak and W. Lotko, On the kinetic dispersion relation for shear Alfvén waves, J. Geophys. Res. **101**, 5085 (1996).

[25] R. L. Lysak, On the dispersion relation for the kinetic Alfvén wave in an inhomogeneous plasma, Phys. Plasmas **15**, 062901 (2008).

[26] B. D. Fried and S. D. Conte, *The Plasma Dispersion Function* (Academic, New York 1961).

[27] W. H. Press, S. A. Teukolsky, W. T. Vetterling, and B. P. Flannery, *Numerical Recipes: The Art of Scientific Computing*, 2nd ed. (Cambridge University Press, Cambridge, England, 1992).

[28] R. W. Ebert, F. Allegrini, F. Bagenal, S. J. Bolton, J. E. P. Connerney, G. Clark *et al.*, Spatial distribution and properties of 0.1–100 keV electrons in Jupiter's polar auroral region, Geophys. Res. Lett. **44**, 9199 (2017).

[29] J. R. Szalay *et al.*, Plasma measurements in the Jovian polar region with Juno/JADE, Geophys. Res. Lett. **44**, 7122 (2017).

[30] B. Zhang, P. A. Delamere, Z. Yao, B. Bonfond, D. Lin, K. A. Sorathia *et al.*, How Jupiter's unusual magnetospheric topology structures its aurora, Sci. Adv. **7**, eabd1204 (2021).

[31] G. Clark *et al.*, Energetic particle signatures of magnetic field-aligned potentials over Jupiter's polar regions, Geophys. Res. Lett. **44**, 8703 (2017).

[32] G. Clark, B. H. Mauk, P. Kollmann, C. Paranicas, F. Bagenal, R. C. Allen *et al.*, Heavy ion charge states in Jupiter's polar

magnetosphere inferred from auroral megavolt electric potentials, J. Geophys. Res. **125**, e2020JA028052 (2020).

[33] F. Bagenal and P. A. Delamere, Flow of mass and energy in the magnetospheres of Juptier and Saturn, J. Geophys. Res. **116**, A05209 (2011).

[34] T. K.-H. Kim, R. W. Ebert, P. W. Valek, F. Allegrini, D. J. McComasm, F. Bagenal *et al.*, Survey of ion properties in Jupiter's plasma sheet: Juno JADE-I observations, J. Geophys. Res. **125**, e2019JA027696 (2020).

[35] Z. Yao, W. R. Dunn, E. E. Woodfield, G. Clark, B. H. Mauk, R. W. Ebert *et al.*, Revealing the source of Jupiter's x-ray auroral flares, Sci. Adv., **7**, eabf0851 (2021).

[36] R. V. Yelle and S. Miller,, Jupiter's thermosphere and ionosphere, in *Jupiter: The Planet, Satellites, and Magnetosphere*, edited by F. Bagenal, T. Dowling, and W. McKinnon (Cambridge University Press, Cambridge, England, 2004), p. 185.

[37] R. W. Schunk and A. F. Nagy, *Ionospheres: Physics, Plasma Physics and Chemistry* (Cambridge University Press 2009), sec. V.7.

[38] D. S. Evans, Precipitating electron fluxes formed by a magnetic field-aligned potential difference, J. Geophys. Res. **79**, 2853 (1974).

[39] J. Dombeck, C. Cattell, N. Prasad, E. Meeker, E. Hanson, and J. McFadden, Identification of auroral electron precipitation mechanism combinations and their relationships to net downgoing energy and number flux, J. Geophys. Res. **123**, 10064 (2018).

[40] The codes, their parameters, and the specific commands used to generated the figures in this Letter are archived at the Data Repository for the University of Minnesota (DRUM), R. L. Lysak (2025), Numerical Codes to solve the dispersion relation for low-frequency waves in Jupiter's polar cap. https://hdl.handle.net/11299/272015. The calibrated Waves (JNO-E/J/SS-WAV-3-CDR-SRVFULL-V2.0) and MAG (JNO-J-3-FGM-CAL-V1.0) data used are from the Planetary Plasma Interactions Node in the Planetary Data System [41,42].

[41] J. E. P. Connerney, Juno MAG CALIBRATED DATA J V1.0, JNO-J-3-FGM-CAL-V1.0. NASA Planetary Data System (2022), 10.17189/1519711.

[42] W. S. Kurth and C. W. Piker, JUNO E/J/S/SS WAVES CALIBRATED SURVEY FULL RESOLUTION V2.0, JNO-E/J/SS-WAV-3-CDR-SRVFULL-V2.0. NASA Planetary Data System (2022), 10.17189/1520498.